Efficiency Analysis of Parasitic Common and Differential Modes for Ultrathin Circularly Polarized Microstrip Antenna

Mingzhe Hu, *Graduate Student Member, IEEE*, Yue Li, *Senior Member, IEEE*, Yongjian Zhang, *Member, IEEE*, Xuan Liu, Pengfei Wu, and Hanyang Wang, *Fellow, IEEE*

***Abstract*— This article proposes a comprehensive analysis on the efficiency performance of an ultrathin circularly polarized (CP) microstrip antenna. For ultrathin antennas with intrinsic narrow bandwidth, traditional parasitic-loading methods for bandwidth enhancement encounter significant in-band efficiency reduction, which is named as "efficiency dip," due to the strong differential coupling between main and parasitic resonators. To address this issue, we propose a feasible structure of parasitic resonator pair. In this case, the common and differential modes (DMs) of the resonator pair are excited simultaneously, with the parasitic common mode (CM) to eliminate the efficiency dip. Inevitably, another efficiency dip appears due to the parasitic DM, but is located out of band without bandwidth deterioration. A prototype is fabricated and tested, showing a CP bandwidth of 3.5% with an extremely low profile of 0.012 λ_0 (λ_0 is the free-space wavelength at the center frequency). The final efficiency is over 68% across the band. This article provides a guideline for designing wideband CP antennas with ultrathin profile and small area, for example, for mobile terminals.**

***Index Terms*— Circular polarization, common mode (CM), differential mode (DM), microstrip antennas, radiation efficiency.**

I. Introduction

MOBILE phones have become indispensable in our lives, offering a wide range of functions beyond basic calls, messaging, and Internet access. For example, ultrawideband (UWB) frequency is with numerous channels spanning from 3.1 to 10.6 GHz. Some subchannels can be used for various applications like indoor positioning due to the advantages of high resolution and multipath immunity [1], [2], [3]. Besides, 5G millimeter-wave applications are also a promising direction for mobile phones [4], with many impressive antenna designs using advanced manufacturing processes [5], [6], [7], [8]. Recently, to improve antenna performance by deploying them out of the bezel, researchers have proposed antennas on the back cover [9], [10], [11], [12] or on the flexible printed circuit (FPC), shown in Fig. 1(a). To integrate with FPC, antennas must have an extremely low profile and limited aperture area. Furthermore, for UWB positioning, circularly polarized (CP) antennas are required to prevent the polarization mismatch. Zhang et al. [13] and Hu et al. [14] demonstrate the feasibility of integrating CP antennas into the FPC, where the profiles are only around 0.6 mm (less than 0.02 λ_0, λ_0 is the free-space wavelength at the center frequency).

With such a low profile, the resonant bandwidth is narrow for a single-operation mode. To achieve a wider bandwidth, three methods are commonly used. The first one employs multiple modes, including the higher-order modes to enhance bandwidth. The most common combination involves a fundamental mode coupled with a higher-order mode [15], [16], [17], [18], [19], [20]. In [15] and [16], TM_{10} mode and antiphase TM_{20} mode are excited and coupled using a gridded patch, while in [18], TM_{10} mode and TM_{30} mode are used. Besides, two higher-order modes can also be used for wideband radiation [21], [22]. Despite the improved bandwidth, the multimode method often requires an enlarged aperture area, which is full of challenges in space-limited environments [23], [24], [25]. The second method uses a feeding network to achieve CP radiation and improve the bandwidth [26], [27], [28], [29], [30], [31], [32]. In [26], a power divider is designed to feed a simple square patch, with bandwidth extended by introducing a quarter- and a half-wavelength resonator in the feeding network. Besides, the sequentially rotated feeding network is well known to provide wideband CP operation [28], [29], [30]. However, the introduction of feeding network complicates the structure and increases the total area. The third method is to use perturbation or parasitic loading [33], [34], [35], [36], [37], [38]. In [33] and [34], two layers of patches create an additional axial ratio (AR) minimum, achieving a 3-dB AR bandwidth of 2.33% and 6%, respectively. In [35], a pair of annular strips is loaded around a slot-perturbed circular patch. By adjusting the length and angle of the strips, AR bandwidth of 3% is obtained with a low profile of

Received 25 October 2024; revised 17 December 2024; accepted 2 January 2025. Date of publication 13 January 2025; date of current version 7 May 2025. This work was supported in part by the National Key Research and Development Program of China under Grant 2021YFA0716601, in part by the National Natural Science Foundation of China under Grant U22B2016, in part by China Postdoctoral Science Foundation under Grant GZB20240334 and Grant 2024M751678, and in part by Huawei Technologies. *(Corresponding author: Yue Li.)*

Mingzhe Hu, Yongjian Zhang, and Xuan Liu are with the Department of Electronic Engineering, Tsinghua University, Beijing 100084, China.

Yue Li is with the State Key Laboratory of Space Network and Communications, Beijing National Research Center for Information Science and Technology, Department of Electronic Engineering, Tsinghua University, Beijing 100084, China (e-mail: lyee@tsinghua.edu.cn).

Pengfei Wu is with the Department of Wireless Technology, Huawei Technology Company Ltd., Shanghai 201206, China (e-mail: wupengfei3@huawei.com).

Hanyang Wang is with Huawei Technologies (U.K.) Ltd., OX14 2HJ Abingdon, U.K. (e-mail: hanyang.wang@huawei.com).

Digital Object Identifier 10.1109/TAP.2025.3526902

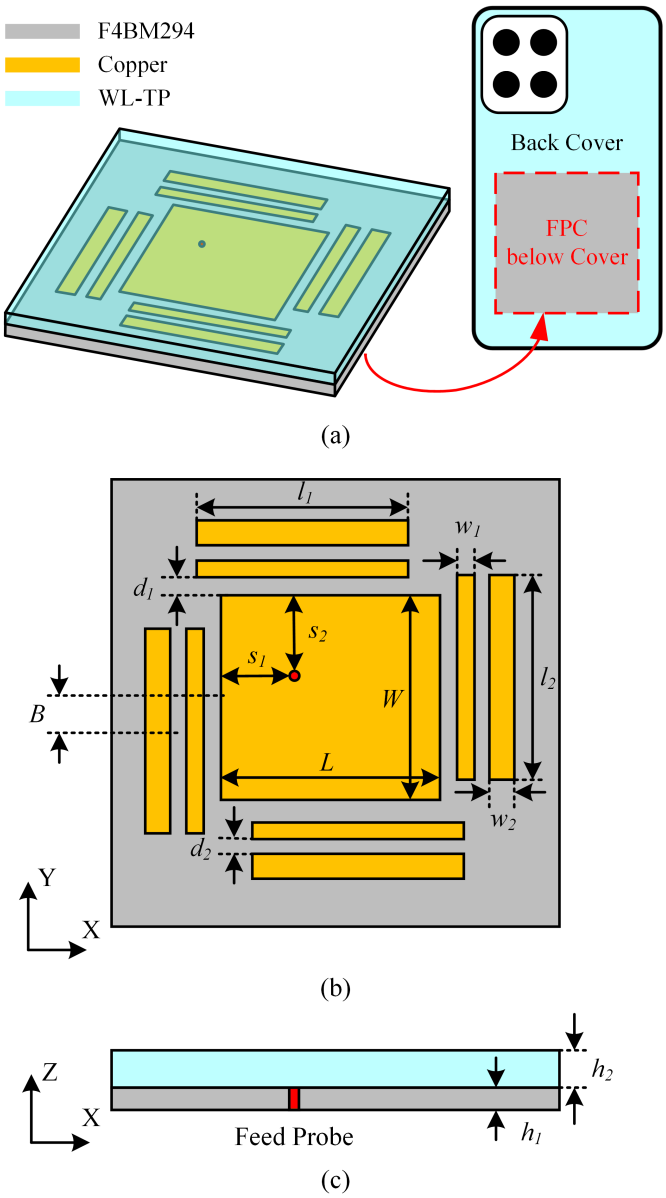

Fig. 1. Configuration of the proposed CP antenna. (a) Application scenario in the mobile phone. (b) Top view of the lower layer. (c) Side view.

only 0.02 λ_0. Similar parasitic structures are also applied in [36], [37], and [38].

Compared with the abovementioned three methods, using parasitic resonators around the main patch achieves enhanced CP bandwidth with a simple and compact structure. In spite of these merits, one significant yet often overlooked issue is the differential coupling between the main and parasitic resonators, leading to efficiency reduction, which is a critical focus in terminal antenna design [39], [40], [41], [42]. In [39], the relationship between the differential coupling of currents and the local efficiency minimum in slot and T-shaped antennas is thoroughly discussed. A similar phenomenon also occurs in microstrip antennas, as in [35] and [36]. In fact, [35] mentions a gain reduction of over 2 dB due to the current cancellation caused by the parasitic annular strips. However, because of their relatively high profiles or compromises during optimization, efficiency is not a major concern in these cases and thus has not been systematically analyzed. However, as the antenna becomes thinner and more compact, the space between main and parasitic resonators decreases. In this scenario, differential coupling causes significant efficiency deterioration, resulting in an unacceptable in-band efficiency dip. Therefore, addressing the efficiency problem is critically important for ultrathin antenna design in mobile terminals.

In this work, we conduct a systematic analysis on the efficiency issue of an ultrathin CP antenna with parasitic loading. Using a simple structure consisting of a rectangular patch loaded with parasitic strips, additional parasitic modes are excited for bandwidth enhancement. However, with such a low profile and small aperture, the efficiency of the parasitic mode is significantly reduced due to the current cancellation. To address this issue, we introduce an additional parasitic strip, forming a parasitic resonator pair. In this configuration, the common mode (CM) and differential mode (DM) of the pair are excited simultaneously. By adjusting the dimensions, the CM is tuned in the operating band, eliminating the original in-band efficiency dip. Meanwhile, the DM which exhibits an obvious efficiency dip appears out of band and thus has no effect on the performance. As a result, the final design achieves high and stable efficiency of over 68% across the operating band, with $S_{11} < -6$ dB and AR < 3 dB. The introduction of the parasitic pair and the parasitic CM/DM provides a feasible solution to ultrathin wideband antenna design with parasitic resonators, showing its potential applications in mobile terminals, such as UWB indoor positioning and Internet of Things applications.

II. Antenna Configuration

Fig. 1 illustrates the structure of the proposed antenna. From the side view shown in Fig. 1(c), the antenna consists of a single-layer substrate and a top layer that simulates the back cover of a mobile phone. The lower substrate is made of F4BM294 with $\varepsilon_r = 2.94$ and $\tan\delta = 0.0016$. It has an extremely low profile of only $h_1 = 0.45$ mm (0.012 λ_0). Above it is a dielectric with a thickness of h_2, made of WL-TP, with $\varepsilon_r = 7$ and $\tan\delta = 0.002$, which has similar electrical properties to the phone's back cover. Fig. 1(b) shows the top view of the antenna. The main structure comprises a rectangular patch and eight parasitic strips arranged around the center patch. The patch has a length of L and a width of W. A single-feed probe is used to excite the patch, with its position finely tuned at distances s_1 and s_2 from the sides. The parasitic strips can be divided into two groups based on their orientation. The x-oriented strips have a length of l_1, while the y-oriented strips have a length of l_2. All four inner strips have a width of w_1, while the four outer strips have a width of w_2. The distance between the strip and the patch is d_1, and the distance between each pair of strips is d_2. The position bias of the stirps is B. The ground plane is printed on the back of the substrate, with a ring cut out for coaxial feed. Detailed dimensions are listed in Table I. Antenna design and optimization are performed using HFSS software.

TABLE I
DETAILED DIMENSIONS (UNIT: MILLIMETERS)

Parameter	Value	Parameter	Value	Parameter	Value
L	9.6	W	9.24	B	1.25
h_1	0.45	l_1	9.2	d_1	0.85
h_2	0.8	l_2	9.26	d_2	0.6
s_1	2.9	w_1	0.8		
s_2	2.8	w_2	1.1		

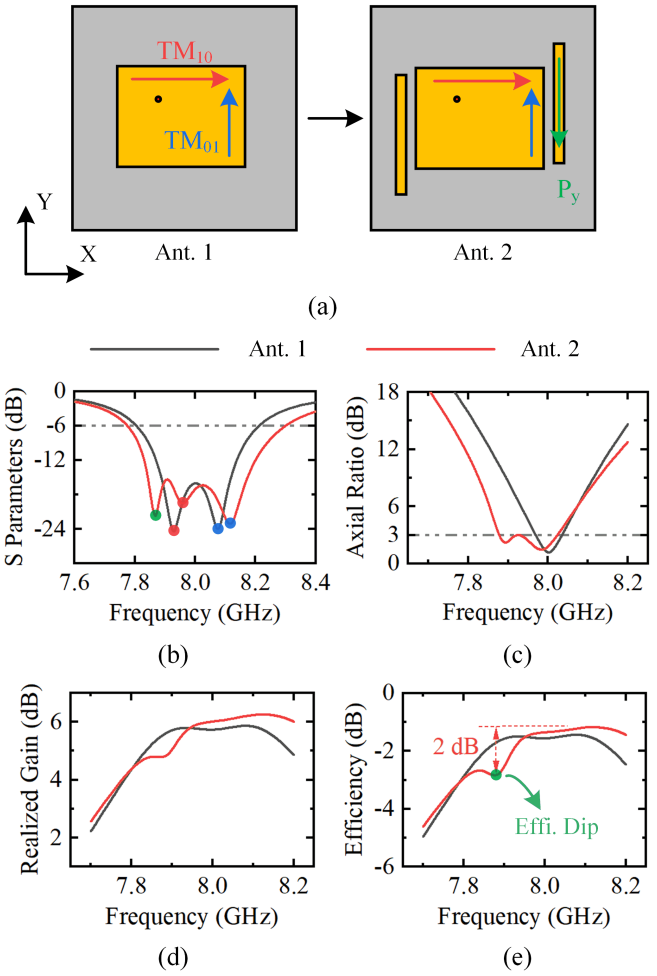

Fig. 2. Comparison of Ant. 1 and Ant. 2. (a) Structural evolution and mode sketch. (b) S-parameter. (c) AR. (d) Realized gain. (e) Efficiency.

III. DESIGN PROCESS

To clarify the working principle of the design, we study the full evolution from a rectangular patch (Ant. 1) to the antenna with four pairs of parasitic strips (Ant. 4). Starting from Ant. 1, CP radiation is achieved due to the degenerated TM_{10} and TM_{01} modes, which are x- and y-polarized, respectively. By adjusting the dimensions of the patch, a 3-dB AR bandwidth of 70 MHz can be achieved. However, the bandwidth is relatively narrow due to the extremely low profile. The gain and efficiency are high, since the two modes can radiate well.

To enhance the CP bandwidth, two parasitic strips are loaded on either side of the central patch along the y-axis (Ant. 2), as shown in Fig. 2(a). The length of the strips can be

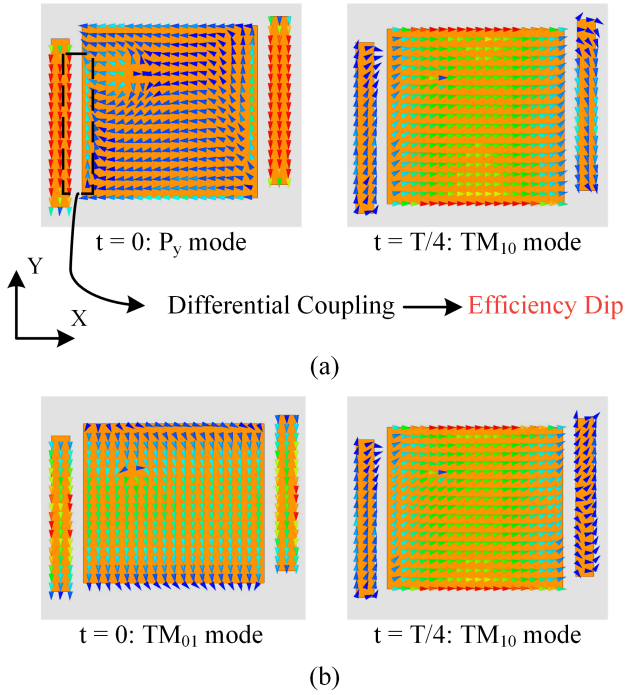

Fig. 3. Current distributions of Ant. 2 at the two AR minima. (a) P_y-TM_{10} modes at 7.9 GHz. (b) TM_{10}-TM_{01} modes at 8 GHz.

finely tuned so that their half-wavelength resonance [referred to as the P_y mode, i.e., y-oriented parasitic mode, plotted green in Fig. 2(a)] has a frequency lower than that of TM_{10} mode. Thus, the combination of P_y-TM_{10}-TM_{01} modes is excited with the adjacent two modes having similar amplitudes and a 90° phase difference. Thus, this configuration can double the CP bandwidth compared to Ant. 1 (140 versus 70 MHz) with two AR minima.

However, as Fig. 2(e) shows, the efficiency at the P_y mode is significantly reduced compared to the two TM modes. Although the reduction is only approximately 2 dB, which may seem acceptable, in realistic environments, however, such as mobile terminals, the losses from the conductor and the surrounding dielectric material may be much higher, causing a deeper and more unpredictable efficiency dip. Therefore, the principles behind the appearance and the solution to the efficiency dip need clarification. From the current distributions plotted in Fig. 3, at 7.9 GHz where the parasitic strips resonate, we observe strong but out-of-phase currents on the patch and the strip, indicating a differential coupling between the two resonators. This coupling mechanism leads to severe current cancellation, causing poor radiation and high loss with an obvious efficiency dip. Notably, as seen in Fig. 2(b) and (e), the decrease in efficiency is not attributed to impedance matching. On the contrary, the reflection coefficient across the band remains well below −6 dB. Thus, the efficiency dip cannot be solved by regular matching technique. Moreover, since the dip is strongly dependent on the resonance of the strip, it is also impossible to separate the dip from the resonance by simply tuning the parameters of the strip. Instead, substantial structural change is needed, which will be shown in the next evolution stage. Meanwhile, the currents at 8 GHz that deviates

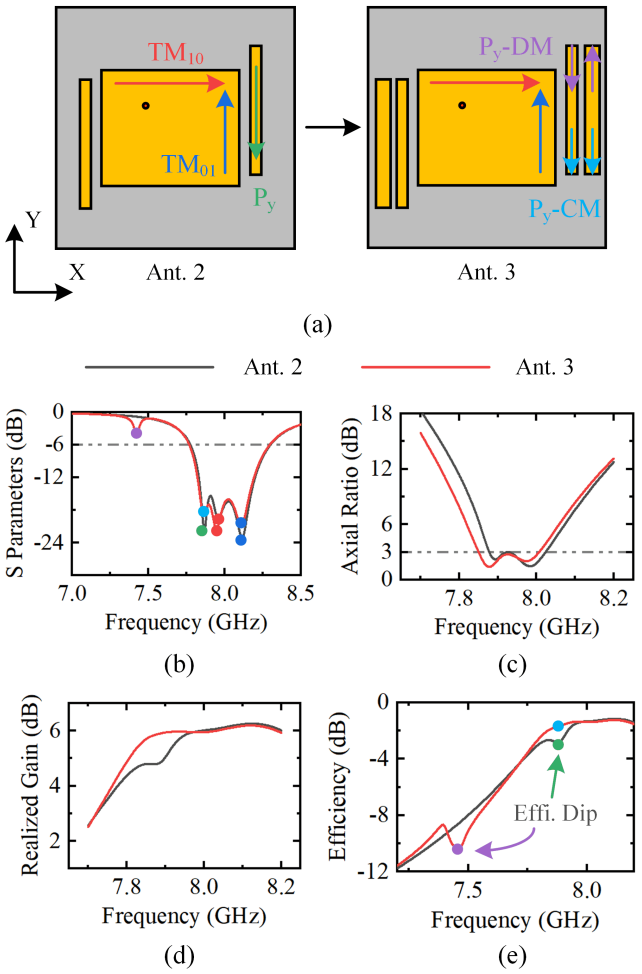

Fig. 4. Comparison of Ant. 2 and Ant. 3. (a) Structural evolution and mode sketch. (b) S-parameter. (c) AR. (d) Realized gain. (e) Efficiency.

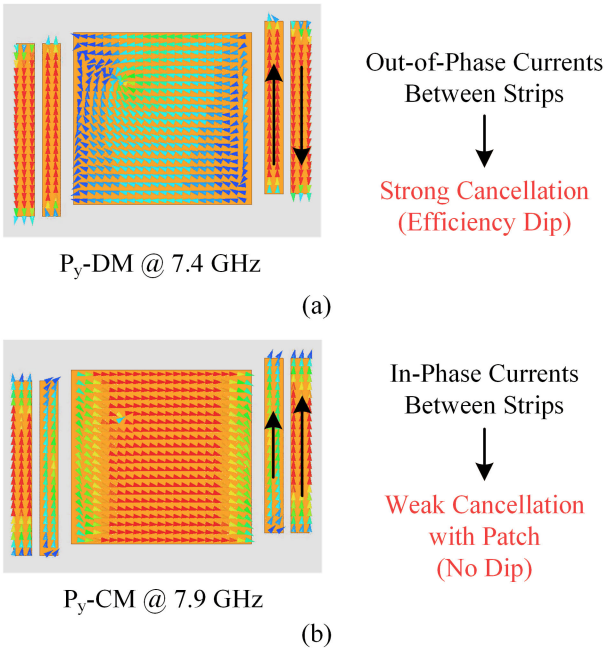

Fig. 5. Current distributions of Ant. 3 at the two parasitic modes. (a) Parasitic DM at 7.4 GHz. (b) Parasitic CM at 7.9 GHz.

from the resonant frequency of the strip are shown in Fig. 3(b), corresponding to the TM_{10}-TM_{01} modes. It can be seen that the currents on the patch and the strips are in the same direction, indicating no current cancellation. Therefore, the efficiency around 8 GHz is not affected by the parasitic strips. In summary, while the parasitic strips expand the bandwidth through differential coupling with the patch, it inevitably causes current cancellation and an efficiency dip at its resonance.

To maintain high and stable efficiency across the entire operating band with the parasitic resonator, we propose a parasitic pair loading technique, which utilizes two strips as a pair instead of the traditional single strip. In this configuration, each y-side of the patch has two strips, forming Ant. 3. According to Fig. 4(b) and (c), both antennas have nearly the same operating bandwidth in terms of S-parameter and AR value. Besides, Ant. 3 has a poor resonance at the low frequency of around 7.3 GHz. Fig. 4(e) illustrates the difference in efficiency between the two designs. Unlike Ant. 2, Ant. 3 has a high and stable efficiency across the operating band, while a significant dip appears out of band, coinciding with the resonance marked purple in Fig. 4(b). The results indicate that Ant. 3 eliminates the original in-band efficiency dip but introduces a new one out of band. To understand its mechanism, we can analyze the current distributions at these two parasitic modes, as shown in Fig. 5. At the lower frequency, which deviates much from the TM_{10} and TM_{01} modes, the patch is not well excited. Instead, the parasitic pair is excited with strong out-of-phase currents, which we refer to as the parasitic DM (P_y-DM, i.e., y-oriented parasitic DM, marked purple). The out-of-phase currents lead to strong cancellation, resulting in an efficiency dip. Nevertheless, it has no effect on the in-band performance. Conversely, at the higher frequency, the pair has currents in the same direction, which we denote as the parasitic CM (P_y-CM, i.e., y-oriented parasitic CM, marked light blue). In this case, the pair acts as a whole with a large radiation aperture. It can also be seen that the two strips both have a differential coupling with the central patch. Besides, the energy is more distributed to the outer strip. Fig. 5(b) shows that the outer strip has much stronger currents. This configuration mitigates the original current cancellation between the patch and the strip, effectively eliminating the efficiency dip. It is noteworthy that, due to the capacitive effect in DM's case, the resonant frequencies of the two parasitic modes are separated. This separation allows one mode to be tuned into the operating band, while keeping the other one out of band. In summary, by loading a pair of strips instead of a single one, two new modes, parasitic CM and DM, are effectively excited, resulting in high in-band efficiency and eliminating the original efficiency dip.

Next, to further expand the bandwidth, we introduce another group of parasitic strips in the orthogonal direction, providing a new resonance (named as the P_x-CM mode, i.e., x-oriented parasitic CM, marked orange in Fig. 6) that is higher than the TM_{01} mode, thereby forming Ant. 4. After optimizing the dimensions of the two pairs of strips and the central patch, a combination of P_y-TM_{10}-TM_{01}-P_x modes can be excited from low to high frequency. Each pair of adjacent modes can produce an AR minimum, summing up to have a wide

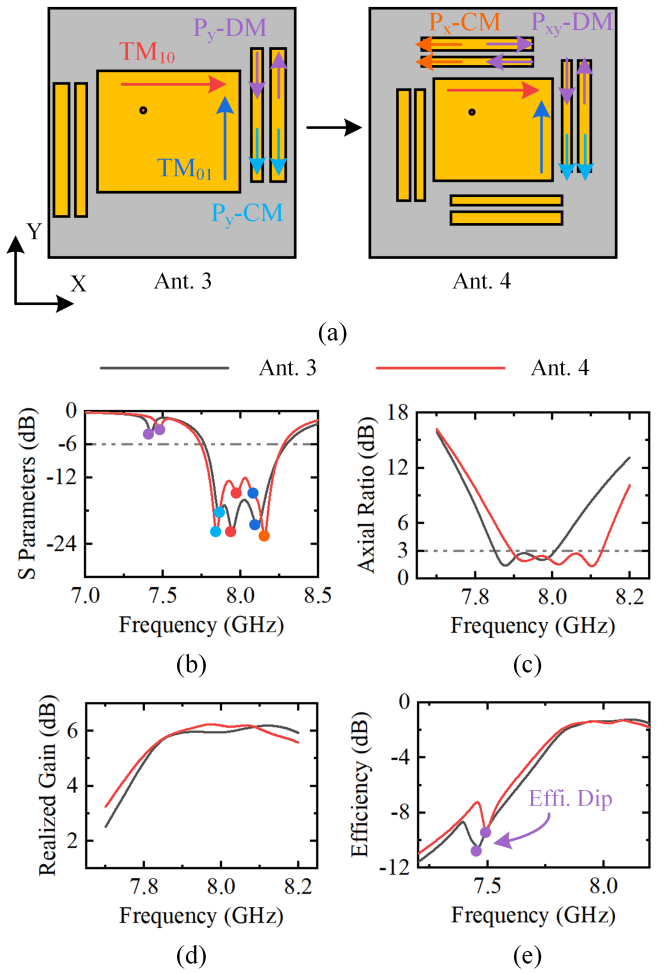

Fig. 6. Comparison of Ant. 3 and Ant. 4. (a) Structural evolution and mode sketch. (b) S-parameter. (c) AR. (d) Realized gain. (e) Efficiency.

CP bandwidth with three AR minima, as shown in Fig. 6. Thanks to the parasitic CM of the pair, the efficiency remains stable across the entire operating band, showing superior performance even in an extremely low profile. As for the parasitic DM, it is noteworthy that Ant. 4 has only one dip outside the band, which is due to the similar lengths of the x- and y-oriented strips and the same distance d_2 between the strips. If we set the parameters with enough difference, there will be two separate dips dependent on the DMs in the two directions, respectively. Here, we combine these two as the parasitic DM (P_{xy}-DM in Fig. 6, marked purple) for brevity. At this mode, the strips both in x- and y-directions have out-of-phase currents in each pair.

To better show the principle of the multiple AR minima, the analysis of E-field is conducted. Fig. 7 shows the amplitude and phase relations between E_θ and E_φ in the broadside direction. In the CP operating band, the amplitudes of E_θ and E_φ are close to 1, while the phase difference fluctuates around 90°. Specifically, the y-oriented and longer strips contribute to E_φ at 7.9 GHz (the first AR minimum), while the x-oriented and shorter strips contribute to E_θ at 8.1 GHz (the third AR minimum). Thus, from low to high frequency, the four modes in the sequence of P_y-TM_{10}-TM_{01}-P_x can be excited to form a wide CP bandwidth with three AR minima.

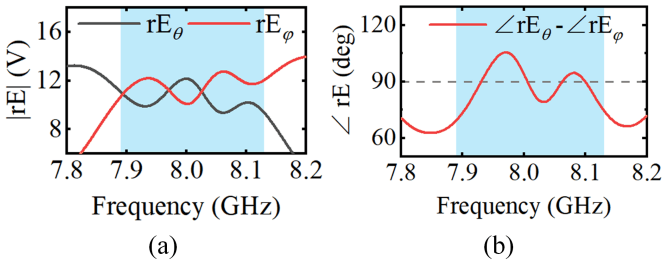

Fig. 7. (a) Amplitudes and (b) phase difference of the two components of E-field at the broadside direction.

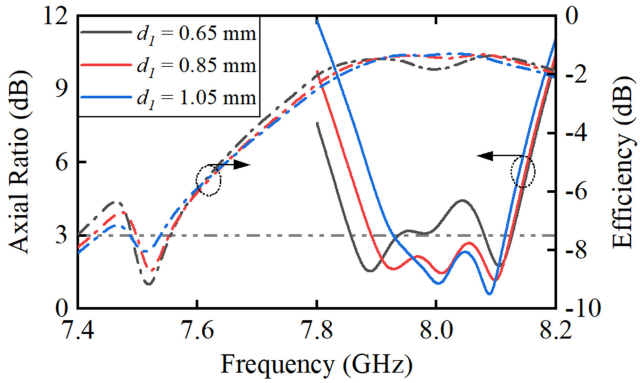

Fig. 8. Parameter study on the distance between the patch and the inner parasitic strip d_1.

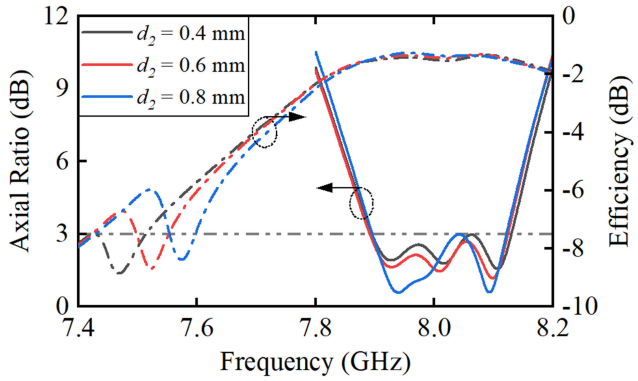

Fig. 9. Parameter study on the distance between the two parasitic strips d_2.

To get a deeper understanding of the parasitic modes, we analyze several key parameters related to the parasitic CM and DM. First, the coupling strength is influenced by the distance between the patch and the pair, denoted as d_1. As shown in Fig. 8, increasing d_1 mitigates the efficiency dip at the parasitic DM, while simultaneously narrowing the CP operating bandwidth. Next, to tune the two parasitic modes independently, we investigate the effect of the distance between the two strips, d_2, as plotted in Fig. 9. The results show that changes in d_2 result in corresponding shifts in the frequency of the efficiency dip, that is, parasitic DM, while in-band parasitic CM remains unaffected. The independent tuning of the two parasitic modes is due to the different distributions of the electric field between the strips. Specifically, the electric field at the DM is tangential to the XoY-plane. Therefore, the distance d_2 mainly influences the capacitive

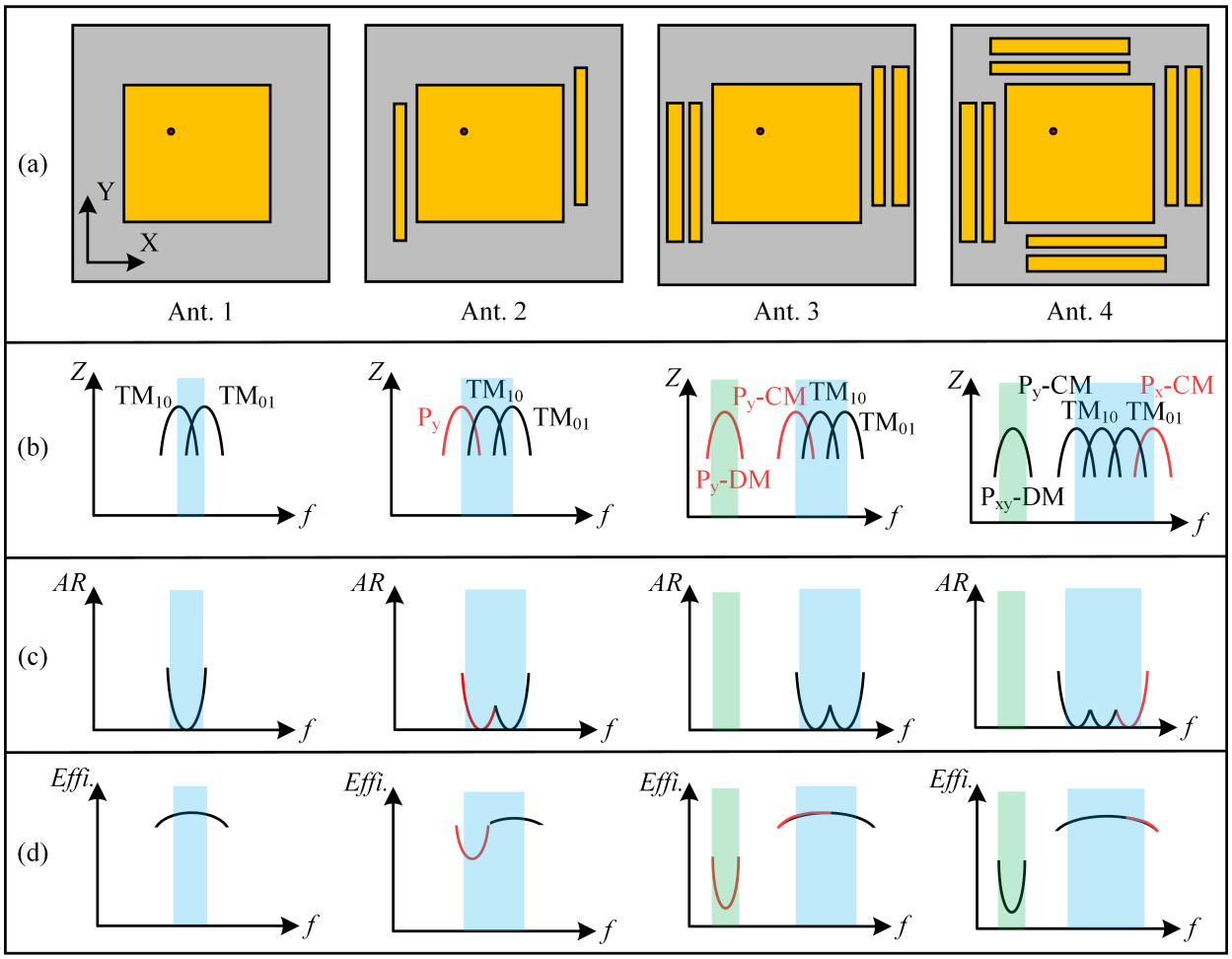

Fig. 10. Summary and design guideline of the proposed antenna. (a) Structural evolution. (b) Impedance and mode distribution. (c) CP performance. (d) Efficiency performance in and outside the operating band.

loading in DM's case. For CM, in contrast, the electric field between the strips is perpendicular to the substrate, with negligible capacitive effects. Thus, by adjusting the length and distance of the parasitic pair, we can control the parasitic CM and DM independently. Apart from these key parameters, other structure settings, such as the bias distance B, the feed position s_1 and s_2 can also be tuned to gain balanced and wideband CP radiation.

To gain a whole picture of the evolution process, we sketch the main performance, including impedance, mode, AR, and efficiency of Ants. 1–4, in Fig. 10. The blue region corresponds to the operating band, while the green one refers to the efficiency dip due to the parasitic DM out of the operating band. To provide a guideline for ultrathin CP antenna design with parasitic structures, it can be summarized as three steps.

1) Start with a rectangular microstrip antenna with its TM_{10} and TM_{01} modes forming circular polarization.
2) Load two pairs of parasitic strips in the same direction, and tune its parasitic CM beside the TM modes to enhance the CP bandwidth. Meanwhile, its parasitic DM is outside the band.
3) Load another two pairs of strips in the other direction to further expand the bandwidth. Adjust the sizes of the patch and the strips for optimized CP performance.

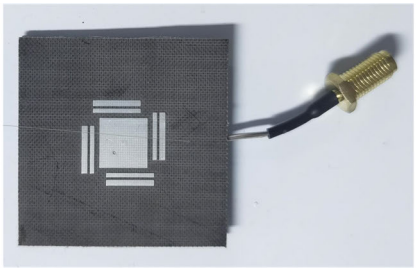

Fig. 11. Fabricated prototype of the proposed antenna. (The top layer is omitted for brevity.)

With the above steps, a wideband high-efficiency CP antenna is elaborately designed for ultrathin scenarios, such as on the back or FPC of mobile terminals.

IV. Results

A prototype of the proposed high-efficiency CP antenna has been fabricated and tested to validate our design. Fig. 11 presents a photograph of the fabricated prototype. A semi-rigid cable is used to feed the antenna, with the inner conductor soldered to the feed probe and the outer one connected to the ground plane. The S-parameters are measured using a vector network analyzer (Agilent N9917A), and the radiation

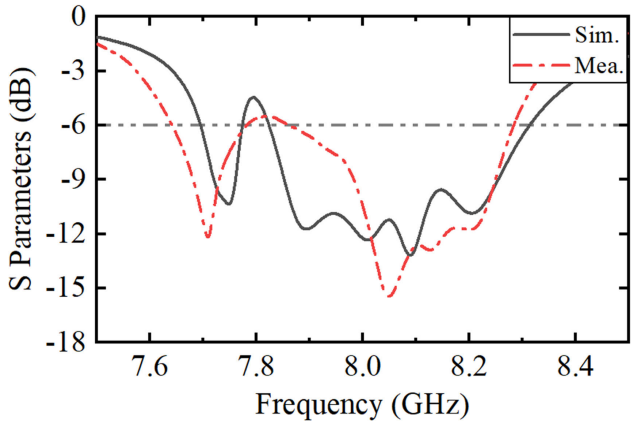

Fig. 12. Simulated and measured S-parameters of the antenna.

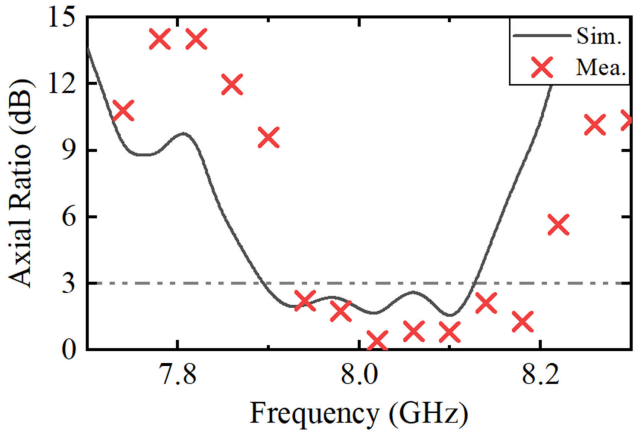

Fig. 13. AR of the antenna.

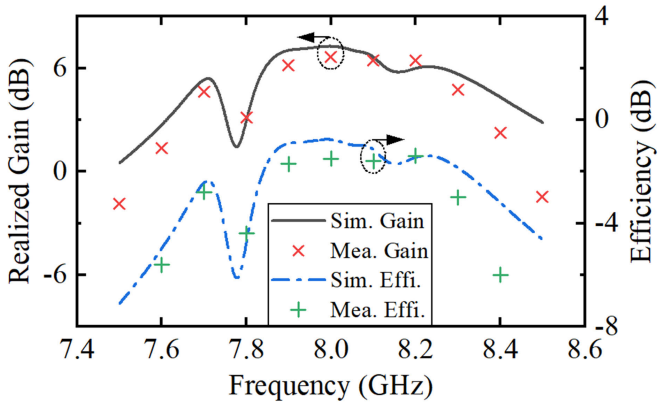

Fig. 14. Realized gain and efficiency of the proposed antenna.

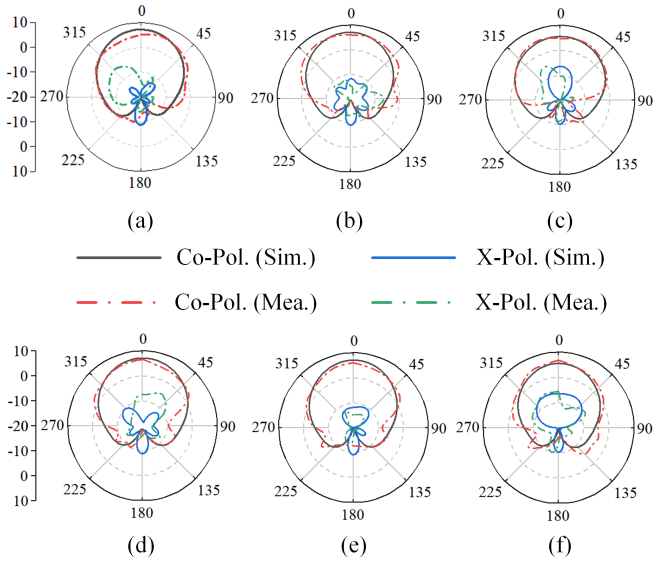

Fig. 15. Radiation patterns of the antenna at (a) 7.95 GHz, (b) 8.05 GHz, (c) 8.15 GHz in XoZ-plane, (d) 7.95 GHz, (e) 8.05 GHz, and (f) 8.15 GHz in YoZ-plane.

properties are measured in an anechoic chamber. The results of S-parameters are shown in Fig. 12. For simulation, the reflection coefficients remain below −6 dB from 7.82 to 8.32 GHz, having a bandwidth of 500 MHz (about 6.2%). It is worth noting that the resonance around 7.7 GHz corresponds to the parasitic DM, which should not be included in the operating band because of its obvious efficiency dip, as is shown later. For measurement, the impedance bandwidth spans from 7.86 to 8.28 GHz (5.2%), which aligns well with simulation. The main difference can be attributed to the actual thickness of the substrate material and other fabrication errors. For CP performance, Fig. 13 displays the AR values of the antenna. The bandwidth with AR < 3 dB is 7.89–8.13 GHz (240 MHz, 3%) in simulation and 7.92–8.2 GHz (280 MHz, 3.5%) in measurement. These results indicate a wide CP bandwidth with multiple AR minima.

Fig. 14 shows the realized gain and efficiency of the antenna. Consistent with the trend observed in AR values, the measured frequencies are slightly higher. Within the working band where $S_{11} < -6$ dB and AR < 3 dB, the realized gain is over 6 dBic, with fluctuations of less than 1 dB. Meanwhile, the efficiency is over 68% (−1.7 dB), indicating that the antenna has properties of high and stable efficiency. The efficiency dip with a reduction of over 4 dB is also observed out of the operating band. Fig. 15 presents the radiation patterns across the band. The low cross-polarization levels mean good CP performance across a wide beam range. Besides, the broadside radiation pattern remains stable throughout the band, beneficial for practical applications such as positioning.

To provide an intuitive comparison with other related low-profile CP antennas, we summarize the main performance metrics in Table II. The operating bandwidth here refers to the combined range where $S_{11} < -6$ dB and AR < 3 dB. Here, we define the ratios of bandwidth-to-profile (B/P) and bandwidth-to-volume (B/V) to evaluate the performance of an ultrathin and compact antenna more intuitively. Among the low-profile designs, ours has the biggest B/P and B/V, showing superior wideband performance in space-limited scenarios. For the works with comparative B/V such as in [33] and [35], a smaller aperture is achieved at the expense of lower gain. On the contrary, our proposed antenna achieves higher gain compared with other antennas with a profile of less than 0.02 λ_0 in [19], [33], [35], [43], and [45], implying well radiation despite the extreme thickness. Besides, the

TABLE II
PERFORMANCE COMPARISON OF LOW-PROFILE CP ANTENNAS

Ref.	Profile (λ_0)	Area (λ_0^2)	Operating Bandwidth	B/P#	B/V*	Gain (dBic)	Efficiency
[19]	0.03	0.58 × 0.56	5%	1.67	0.52	4.5	90%
[26]	0.04	0.50 × 0.39	6.2%	1.55	0.79	7.0	90%
[35]	0.016	0.50× 0.27	3.3%	2.06	1.53	2.7	N. G.
[43]	0.013	0.29 × 0.29	0.93%	0.72	0.85	3.9	N. G.
[45]	0.028	0.46 × 0.23	1.2%	0.43	0.41	4.0	N. G.
Proposed	**0.012**	0.43 × 0.42	3.5%	**2.92**	**1.62**	**7.0**	84%

B/P: Bandwidth-to-profile ratio, unit: %/10^{-2} λ_0; * B/V: Bandwidth-to-volume ratio, unit: %/10^{-3} λ_0^3; N. G.: not given

proposed antenna adopts a single-layer substrate, which is easy to fabricate and shows potential to be even thinner. Compared to other methods, such as multimode coupling in [19] and [20] or using feeding network in [26] and [44], our design achieves a smaller aperture, beneficial for integration in mobile terminals. Moreover, the novel parasitic resonator pair also addresses the efficiency and gain reduction encountered in [35], providing high-efficiency performance across the band. The merits in profile, aperture, and comprehensive analysis of efficiency make the proposed antenna particularly feasible for ultrathin environments, such as the back cover or FPC of mobile terminals.

V. CONCLUSION

In this article, we conduct a comprehensive analysis of the efficiency performance of the ultrathin CP microstrip antenna. By examining the current distributions, we discuss the principles of appearance and elimination of the in-band efficiency dip. Specifically, the differential coupling between the main and parasitic resonators causes efficiency reduction. Furthermore, by loading parasitic resonator pair, the parasitic CM and DM can be excited at the same time, with CM to eliminate the in-band efficiency dip, and DM, despite its inevitable low efficiency, out of the operating band. Applying four parasitic pairs, we design an ultrathin wideband CP antenna with a compact area of $0.43 \times 0.42 \times 0.012\ \lambda_0^3$. Measured results show that the antenna achieves an impedance bandwidth of 420 MHz (5.2%) with $S_{11} < -6$ dB and a CP bandwidth of 280 MHz (3.5%) with AR < 3 dB. The realized gain in the operating band is over 6 dBic, with an efficiency of over 68%. With its ultrathin profile, compact size, enhanced CP bandwidth, and high in-band efficiency, the antenna exhibits its superiority in ultrathin configurations, such as FPC in the back of mobile terminals, for various UWB applications.

REFERENCES

[1] A. Yassin et al., "Recent advances in indoor localization: A survey on theoretical approaches and applications," *IEEE Commun. Surveys Tuts.*, vol. 19, no. 2, pp. 1327–1346, 2nd Quart., 2017.

[2] H. Liu, H. Darabi, P. Banerjee, and J. Liu, "Survey of wireless indoor positioning techniques and systems," *IEEE Trans. Syst., Man, Cybern. C, Appl. Rev.*, vol. 37, no. 6, pp. 1067–1080, Nov. 2007.

[3] F. Zafari, A. Gkelias, and K. K. Leung, "A survey of indoor localization systems and technologies," *IEEE Commun. Surveys Tuts.*, vol. 21, no. 3, pp. 2568–2599, 3rd Quart., 2019.

[4] J. G. Andrews et al., "What will 5G be?" *IEEE J. Sel. Areas Commun.*, vol. 32, no. 6, pp. 1065–1082, Jun. 2014.

[5] H. Li, Y. Li, L. Chang, W. Sun, X. Qin, and H. Wang, "A wideband dual-polarized endfire antenna array with overlapped apertures and small clearance for 5G millimeter-wave applications," *IEEE Trans. Antennas Propag.*, vol. 69, no. 2, pp. 815–824, Feb. 2021.

[6] H. Li, Z. Zhou, Y. Zhao, and Y. Li, "Low-loss beam synthesizing network based on epsilon-near-zero (ENZ) medium for on-chip antenna array," *Chip*, vol. 2, no. 2, Jun. 2023, Art. no. 100049.

[7] Y. Zhu and C. Deng, "Wideband dual-polarized endfire phased array antenna with small ground clearance for 5G mmWave mobile terminals," *IEEE Trans. Antennas Propag.*, vol. 71, no. 6, pp. 5469–5474, Jun. 2023.

[8] J. Park, I. Jang, B. Seong, and W. Hong, "Differentially fed, 1-D phased-array antenna-on-display featuring wideband and polarization agility for millimeter-wave wireless applications," *IEEE Trans. Antennas Propag.*, vol. 71, no. 9, pp. 7196–7205, Sep. 2023.

[9] L. Chang and H. Wang, "Miniaturized wideband four-antenna module based on dual-mode PIFA for 5G 4×4 MIMO applications," *IEEE Trans. Antennas Propag.*, vol. 69, no. 9, pp. 5297–5304, Sep. 2021.

[10] M. Hu and Y. Li, "Wideband back cover microstrip antenna with multiple shorting vias for mobile 5G MIMO applications," *IEEE Trans. Antennas Propag.*, vol. 71, no. 10, pp. 8290–8295, Oct. 2023.

[11] S. Gao, L. Chang, A. Zhang, Y. Li, and Z. Zhang, "Small-volume microstrip patch antennas exactly covering Wi-Fi 6 bands of 2.4–2.5 GHz and 5.15–5.85 GHz," *IEEE Trans. Antennas Propag.*, vol. 71, no. 7, pp. 5739–5748, Jul. 2023.

[12] M. Chen, L. Chang, and A. Zhang, "Wideband antenna pairs consisting of E-/M-coupling frame monopoles and M-/E-coupling back cover patches for mobile terminal applications," *IEEE Trans. Antennas Propag.*, vol. 72, no. 2, pp. 1308–1318, Feb. 2024.

[13] Y. Zhang, Y. Li, M. Hu, P. Wu, and H. Wang, "Dual-band circular-polarized microstrip antenna for ultrawideband positioning in smartphones with flexible liquid crystal polymer process," *IEEE Trans. Antennas Propag.*, vol. 71, no. 4, pp. 3155–3163, Apr. 2023.

[14] M. Hu, Y. Li, Y. Zhang, P. Wu, and H. Wang, "Ultrathin dual-band circularly polarized antenna," *IEEE Antennas Wireless Propag. Lett.*, vol. 23, pp. 930–934, 2024.

[15] W. E. I. Liu, Z. N. Chen, and X. Qing, "Broadband circularly polarized metasurface antenna fed by a rotated L-shaped probe," in *Proc. 14th Eur. Conf. Antennas Propag. (EuCAP)*, Copenhagen, Denmark, Mar. 2020, pp. 1–4.

[16] W. Sun, Y. Li, Z. Zhang, and P.-Y. Chen, "Low-profile and wideband microstrip antenna using quasi-periodic aperture and slot-to-CPW transition," *IEEE Trans. Antennas Propag.*, vol. 67, no. 1, pp. 632–637, Jan. 2019.

[17] W. Hu et al., "Wideband circularly polarized microstrip patch antenna with multimode resonance," *IEEE Antennas Wireless Propag. Lett.*, vol. 20, no. 4, pp. 533–537, Apr. 2021.

[18] N.-W. Liu, L. Zhu, and W.-W. Choi, "A differential-fed microstrip patch antenna with bandwidth enhancement under operation of TM_{10} and TM_{30} modes," *IEEE Trans. Antennas Propag.*, vol. 65, no. 4, pp. 1607–1614, Apr. 2017.

[19] N.-W. Liu, L. Zhu, Z.-X. Liu, G. Fu, and Y. Liu, "Design approach of a single circularly polarized patch antenna with enhanced AR-bandwidth under triple-mode resonance," *IEEE Trans. Antennas Propag.*, vol. 68, no. 8, pp. 5827–5834, Aug. 2020.

[20] J. Zeng, X. Liang, L. He, F. Guan, F. H. Lin, and J. Zi, "Single-fed triple-mode wideband circularly polarized microstrip antennas using characteristic mode analysis," *IEEE Trans. Antennas Propag.*, vol. 70, no. 2, pp. 846–855, Feb. 2022.

[21] Y. Zhang and Y. Li, "Wideband microstrip antenna in small volume without using fundamental mode," *Electromagn. Sci.*, vol. 1, no. 2, Jun. 2023, Art. no. 0020073.

[22] Y. He, Y. Li, W. Sun, and Z. Zhang, "Dual-polarized, high-gain, and low-profile magnetic current array antenna," *IEEE Trans. Antennas Propag.*, vol. 67, no. 2, pp. 1312–1317, Feb. 2019.

[23] Y. Zhang, Y. Li, W. Zhang, Z. Zhang, and Z. Feng, "Omnidirectional antenna diversity system for high-speed onboard communication," *Engineering*, vol. 11, pp. 72–79, Apr. 2022.

[24] Y. Zhang, P. Li, X. Qin, P. Liang, K. Wei, and Y. Li, "Dual-polarized microstrip antenna with single-dimension-constraint resonant frequency," *IEEE Trans. Antennas Propag.*, vol. 72, no. 11, pp. 8365–8374, Nov. 2024.

[25] P. Li, Y. Zhang, X. Qin, K. Wei, P. Liang, and Y. Li, "Wideband wide-beam circular-polarized antenna using asymmetrical tri-dipoles for direct satellite-to-handset communications," *IEEE Trans. Antennas Propag.*, vol. 72, no. 8, pp. 6270–6277, Aug. 2024.

[26] Q.-S. Wu, X. Zhang, and L. Zhu, "A wideband circularly polarized patch antenna with enhanced axial ratio bandwidth via co-design of feeding network," *IEEE Trans. Antennas Propag.*, vol. 66, no. 10, pp. 4996–5003, Oct. 2018.

[27] K.-L. Wong and T.-W. Chiou, "Broad-band single-patch circularly polarized microstrip antenna with dual capacitively coupled feeds," *IEEE Trans. Antennas Propag.*, vol. 49, no. 1, pp. 41–44, Jan. 2001.

[28] S.-K. Lin and Y.-C. Lin, "A compact sequential-phase feed using uniform transmission lines for circularly polarized sequential-rotation arrays," *IEEE Trans. Antennas Propag.*, vol. 59, no. 7, pp. 2721–2724, Jul. 2011.

[29] Q. Liu, Y. Liu, Y. Wu, M. Su, and J. Shen, "Compact wideband circularly polarized patch antenna for CNSS applications," *IEEE Antennas Wireless Propag. Lett.*, vol. 12, pp. 1280–1283, 2013.

[30] S. X. Ta and I. Park, "Compact wideband circularly polarized patch antenna array using metasurface," *IEEE Antennas Wireless Propag. Lett.*, vol. 16, pp. 1932–1936, 2017.

[31] J. Wu, X. Ren, Z. Wang, and Y. Yin, "Broadband circularly polarized antenna with L-shaped strip feeding and shorting-pin loading," *IEEE Antennas Wireless Propag. Lett.*, vol. 13, pp. 1733–1736, 2014.

[32] V. Paul and K. Dhwaj, "A reflectionless circularly polarized high-gain microstrip filtering antenna with wideband response," *IEEE Trans. Antennas Propag.*, vol. 72, no. 6, pp. 5384–5389, Jun. 2024.

[33] M.-C. Tang, X. Chen, M. Li, and R. W. Ziolkowski, "A bandwidth-enhanced, compact, single-feed, low-profile, multilayered, circularly polarized patch antenna," *IEEE Antennas Wireless Propag. Lett.*, vol. 16, pp. 2258–2261, 2017.

[34] Z.-X. Liu, L. Zhu, and X. Zhang, "A low-profile and high-gain CP patch antenna with improved AR bandwidth via perturbed ring resonator," *IEEE Antennas Wireless Propag. Lett.*, vol. 18, no. 2, pp. 397–401, Feb. 2019.

[35] J. Lin and Q. Chu, "Enhancing bandwidth of CP microstrip antenna by using parasitic patches in annular sector shapes to control electric field components," *IEEE Antennas Wireless Propag. Lett.*, vol. 17, no. 5, pp. 924–927, May 2018.

[36] J. Wu, Y. Yin, Z. Wang, and R. Lian, "Broadband circularly polarized patch antenna with parasitic strips," *IEEE Antennas Wireless Propag. Lett.*, vol. 14, pp. 559–562, 2015.

[37] K. Ding, C. Gao, D. Qu, and Q. Yin, "Compact broadband circularly polarized antenna with parasitic patches," *IEEE Trans. Antennas Propag.*, vol. 65, no. 9, pp. 4854–4857, Sep. 2017.

[38] Y. Dong et al., "Broadband circularly polarized filtering antennas," *IEEE Access*, vol. 6, pp. 76302–76312, 2018.

[39] K. Liu, D. Yu, and H. Wang, "Investigation on the radiation efficiency local minimum in open-slot and T-shaped antennas," *IEEE Trans. Antennas Propag.*, vol. 69, no. 9, pp. 5257–5268, Sep. 2021.

[40] Y. Luo, L. Zhu, Y. Liu, Y. Xu, N. Liu, and S. Gong, "Efficiency improvement of smartphone antennas using higher-order mode suppression under characteristic mode analysis," *IEEE Trans. Antennas Propag.*, vol. 70, no. 11, pp. 10304–10317, Nov. 2022.

[41] H. Li, M. Wu, W. Li, and Y. Yu, "Reducing hand effect on mobile handset antennas by shaping radiation patterns," *IEEE Trans. Antennas Propag.*, vol. 69, no. 8, pp. 4279–4288, Aug. 2021.

[42] M. Yi Liang et al., "High head–hand efficiency and low-sar mobile phone antenna design based on unidirectional and uniform current distribution," *IEEE Trans. Antennas Propag.*, vol. 72, no. 7, pp. 5560–5568, Jul. 2024.

[43] M. K. Ray, K. Mandal, and N. Nasimuddin, "Low-profile circularly polarized patch antenna with wide 3 dB beamwidth," *IEEE Antennas Wireless Propag. Lett.*, vol. 18, no. 12, pp. 2473–2477, Dec. 2019.

[44] W.-J. Yang, Y.-M. Pan, and X.-Y. Zhang, "A single-layer low-profile circularly polarized filtering patch antenna," *IEEE Antennas Wireless Propag. Lett.*, vol. 20, no. 4, pp. 602–606, Apr. 2021.

[45] N.-W. Liu, M.-J. Sun, L. Zhu, Z.-X. Liu, L. Yang, and L.-Y. Ji, "A single-layer single-fed shorted-patch antenna with broadside circular polarization by using nondegenerate $TM_{0,1/2}$ and $TM_{1,1/2}$ modes," *IEEE Antennas Wireless Propag. Lett.*, vol. 19, no. 6, pp. 939–943, Jun. 2020.

Mingzhe Hu (Graduate Student Member, IEEE) received the B.S. degree in electronic engineering from Tsinghua University, Beijing, China, in 2022, where he is currently pursuing the Ph.D. degree in electronic engineering.

His current research interests include wideband antennas, low-profile antennas, and microstrip antennas.

Mr. Hu serves as a reviewer for the IEEE TRANSACTIONS ON ANTENNAS AND PROPAGATION, IEEE ANTENNAS AND WIRELESS PROPAGATION LETTERS, and *Microwave and Optical Technology Letters*.

Yue Li (Senior Member, IEEE) received the B.S. degree in telecommunication engineering from Zhejiang University, Hangzhou, Zhejiang, China, in 2007, and the Ph.D. degree in electronic engineering from Tsinghua University, Beijing, China, in 2012.

In June 2012, he was a Post-Doctoral Fellow with the Department of Electronic Engineering, Tsinghua University. In December 2013, he was a Research Scholar with the Department of Electrical and Systems Engineering, University of Pennsylvania, Philadelphia, PA, USA. He was also a Visiting Scholar with the Institute for Infocomm Research (I2R), A*STAR, Singapore, in 2010, and Hawaii Center of Advanced Communication (HCAC), University of Hawaii at Manoa, Honolulu, HI, USA, in 2012. Since January 2016, he has been with Tsinghua University, where he is currently an Assistant Professor and an Associate Professor with the Department of Electronic Engineering. He has authored and co-authored over 260 journal articles and 50 international conference papers. He holds 26 granted Chinese patents. His current research interests include metamaterials, plasmonics, electromagnetics, nanocircuits, mobile and handset antennas, MIMO and diversity antennas, and millimeter-wave antennas and arrays.

Dr. Li was a recipient of the Issac Koga Gold Medal from URSI General Assembly. He served as an Associate Editor for IEEE TRANSACTIONS ON ANTENNAS AND PROPAGATION and IEEE ANTENNAS AND WIRELESS PROPAGATION LETTERS from 2017 to 2024. He is also serving as an Associate Editor for *Microwave and Optical Technology Letters* and *Computer Applications in Engineering Education*.

Yongjian Zhang (Member, IEEE) received the B.S. degree in communication engineering from Tongji University, Shanghai, China, in 2018, and the Ph.D. degree in electronic engineering from Tsinghua University, Beijing, China, in 2023.

He is currently a Post-Doctoral Fellow with the Department of Electronic Engineering, Tsinghua University. His current research interests include aircraft antennas, dual-polarized antennas, and multiple-input and multiple-output (MIMO) antenna arrays.

Dr. Zhang serves as a reviewer for the IEEE TRANSACTIONS ON ANTENNAS AND PROPAGATION, IEEE ANTENNAS AND WIRELESS PROPAGATION LETTERS, and *Microwave and Optical Technology Letters*.

Xuan Liu was born in Yulin, Shaanxi, China, in 1999. He received the B.S. degree in electronic engineering from Xidian University, Xi'an, China, and the M.S. degree from Beihang University, Beijing, China. He is currently pursuing the Ph.D. degree in electronic engineering with Tsinghua University, Beijing.

His research interests include on-chip antenna design, antenna-in-package solutions, and low-profile microstrip antenna design.

Pengfei Wu received the B.S. and M.S. degrees from Southeast University, Nanjing, China, in 2005 and 2008, respectively.

From 2009 to 2011, he was an RF Engineer to design antennas with Nokia Mobile, Amphenol, Finland. From 2012 to 2015, he joined ZTE, Shenzhen, China, as a Senior RF Engineer. He is currently an Antenna Specialist with the Consumer Business Group, Huawei Technology Company, Ltd., Shanghai, China. His current research interests include broadband antennas, multiple-input multiple-output antennas, and low-profile antennas.

Hanyang Wang (Fellow, IEEE) received the Ph.D. degree from Heriot-Watt University, Edinburgh, U.K., in 1995.

From 1986 to 1991, he served as a Lecturer and an Associate Professor with Shandong University, Jinan, China. From 1995 to 1999, he was a Post-Doctoral Research Fellow with the University of Birmingham, Birmingham, U.K., and the University of Essex, Colchester, U.K. From 1999 to 2000, he was with Vector Fields Ltd., Oxford, U.K., as a Software Development and Microwave and Antenna Engineering Consultant Engineer. He joined Nokia U.K. Ltd., Farnborough, U.K., in 2001, where he had been a Mobile Antenna Specialist for 11 years. He was an Adjunct Professor at Nanjing University, Nanjing, China, from 2019 to 2022. He joined Huawei after leaving Nokia U.K. Ltd., where he is currently the Chief Scientist of mobile terminal antennas. He leads a large group of antenna experts and engineers and takes the full leadership and responsibility in the research and development of antenna technologies to guarantee the market success of all Huawei's mobile terminal products ranging from smartphones, laptops, tablets, MiFi, data cards, smart watches, BT headsets, routers, IoT, smart screens, CPE, VR, automobiles. He has been an Adjunct Professor at Sichuan University, Chengdu, China, since 2011. He has authored over referred 160 papers on these topics. He holds over 100 granted US/EU/JP/CN patents, including 50 US patents, and has other 100+ patent applications in pending. His current research interests include small, wideband, multiband antennas and MIMO antennas for mobile terminals, and antenna arrays for 5G sub-6GHz and 5G millimeter wave mobile communications.

Dr. Wang is a Huawei Fellow and an IET Fellow. He was a recipient of the Title of Nokia Inventor of the Year in 2005, the Nokia Excellence Award in 2011, the Huawei Individual Gold Medal Award in 2012, and the Huawei Team Gold Medal Award in 2013 and 2014, respectively. His patent was ranked number one among 2015 Huawei top ten patent awards. He was an Associate Editor of the IEEE ANTENNAS AND WIRELESS PROPAGATION LETTERS from 2015 to 2021.